

Superresolution-focal-volume induced 3.0 Tbytes/disk capacity by focusing a radially polarized beam

Xiangping Li, Yaoyu Cao, and Min Gu*

Centre for Micro-Photonics, Faculty of Engineering and Industrial Sciences,
Swinburne University of Technology, P.O. Box 218, Hawthorn, Victoria 3122, Australia

*Corresponding author: mgu@swin.edu.au

Received April 12, 2011; revised June 2, 2011; accepted June 3, 2011;
posted June 3, 2011 (Doc. ID 145672); published June 24, 2011

This paper reports on the study of the superresolution volume of the focal spot by focusing a radially polarized beam. This feature is achieved by increasing the inner radius of a high NA annular objective to break the diffraction-limited volume of a focal spot. The application of this finding into two-photon induced three-dimensional optical data storage leads to an enhanced photoreduction threshold effect in recording. As such, multilayer subdiffraction optical recording is experimentally demonstrated with an equivalent capacity of 3.0 Tbytes/disk. © 2011 Optical Society of America

OCIS codes: 210.4680, 210.4770, 100.6640.

The ever increasing demand of more data storage capacity compels the development of high density optical data storage techniques including two-photon (2P) induced three-dimensional (3D) recording [1]. In the last two decades, 2P excitation has been widely adopted for 3D bit-by-bit optical data storage in various erasable and nonerasable mechanisms [2–6]. However, the capacity of 3D optical data storage is limited by the diffraction nature of the light as $r = 0.61 \times \lambda/\text{NA}$, where λ is the wavelength and NA is the numerical aperture of the lens [7]. The theory predicts a storage density limit of a few Tbits/cm³ of an objective of NA = 1.4 [8]. By exploring the unique optical properties of functional materials, encoding information in the polarization and spectral domain of the writing beam has been demonstrated with an increased storage capacity [9–11].

An alternative approach to increase the storage density is to break the diffraction limited barrier and achieve a superresolution recording nature. Owing to the vectorial property of the beam inside the focus, it has been predicted that it is possible to achieve a far-field extremely tight focus spot when a special polarization pattern is used [12]. It has been shown when focusing by an objective of large NA, the radially polarized beam leads to a strong longitudinal electric field, the lateral size of which is smaller than the diffraction limit [12,13]. The relative strength of the longitudinal component can be enhanced by changing the annular aperture [14] or using the diffractive optical element [15], therefore enabling a superresolution lateral focal spot. However, for the application of such a far-field subdiffraction focusing technique in 3D optical data storage, a superresolution volume rather than the lateral size of the focal spot produced by a high NA objective determines the storage capacity, which has never been explored yet. In this Letter, we reported on the study of the superresolution volume of the focal spot facilitated by increasing the obstruction size of the annular aperture and its application in 2P induced multilayer optical memory in a photoreduction polymer.

Let us consider a high NA objective with an annular aperture of inner and outer radii d_1 and d_2 , respectively.

The electric field components inside the focus of a radially polarized beam by the objective can be expressed as [13]

$$E_r(r, z) = A \int_b^a \cos^{1/2} \theta \cdot \sin(2\theta) \cdot J_1(kr \sin \theta) e^{ikz \cos \theta} d\theta, \quad (1)$$

$$E_z(r, z) = 2iA \int_b^a \cos^{1/2} \theta \cdot \sin^2 \theta \cdot J_0(kr \sin \theta) e^{ikz \cos \theta} d\theta, \quad (2)$$

where E_r and E_z are the radial and longitudinal components, respectively. $a = \arcsin(\text{NA}/n)$ is the maximum angle of the convergence for the high NA objective, and n is the refractive index of the media. $b = \arcsin(\varepsilon \times \text{NA}/n)$, where $\gamma = d_1/d_2$ is defined as the ratio of inner to outer radii of the annular objective. For the calculation, the experimental condition of NA = 1.4 and $n = 1.49$ (refractive-index of Poly(methyl methacrylate) (PMMA) at the wavelength of 800 nm) [16] was applied. It has been shown that the lateral size of the longitudinal electric field is much narrower than the diffraction limit [12,14]. This is clear when the lateral area and the axial FWHM of the focal spot are plotted as a function of γ in Fig. 1(a). The calculation by the vectorial Debye theory predicts the smallest lateral FWHM by increasing the γ at 0.41λ or lateral area of $0.135\lambda^2$, which is significantly sharper than the diffraction limited lateral area of $0.232\lambda^2$ and is consistent with previous reports [14,15].

For the 3D recording, the focal volume is of significance. The theoretical storage density limit is mainly confined by the volume of the focal spot, V , which can be expressed as [8]

$$V = \frac{4\pi}{3} (\Delta r)^2 \Delta z, \quad (3)$$

where Δr and Δz are the FWHMs of the lateral and axial dimensions of a focal spot, respectively. The volume of the focal spot and the theoretical storage density limit are

plotted as a function of γ in Fig. 1(b). It depicts clearly that the superresolution volume of the focal spot of $2.28\lambda^3$ can be achieved by balancing the reduction in the lateral size and elongation in the axial size, therefore leading to a peak storage density of $0.436\lambda^{-3}$ when the optimized annular aperture $\gamma = 0.65$ is adopted, where λ is the wavelength inside the recording media. This result predicts a 129% increase in the theoretical storage density limit compared to that confined by the diffraction limited Airy focal spot of an objective of NA = 1.4, where the storage density limit is calculated to be $0.19\lambda^{-3}$ [7].

In addition, the superresolution focal volume (SFV) can lead to an enhanced power density inside the focus, therefore significantly strengthening the threshold sensitivity in optical recording. This was confirmed by the recording when opaque disks of different sizes were coaxially placed in the back aperture of the objective, as illustrated in Fig. 1(c). Owing to its high photosensitivity [17], a photoreduction polymer consisting of 16 mg of HAuCl₄, 0.67 mg of R6G, and 570 mg of PMMA was prepared. A femtosecond pulsed laser at the wavelength of 800 nm was employed as the 2P excitation source. The radially polarized beam was converted by the twisted nematic liquid crystal device (Arcoptix S.A.) [18]. An objective of NA = 1.4 was used to focus the radially polarized beam into the recording media to introduce the photoreduction of Au ions into nanoparticles. Figures 2(a) and 2(b) show the absorption and fluorescence evolution of the sample before and after the irradiation, respectively. The broad absorption from 400 to 1000 nm arises due to the generated Au nanoparticles after the laser illumination. The fluorescence is emitted from R6G dyes by 2P excitation, which is collected by a CCD camera. Because of the large 2P absorption cross sections of Au nanoparticles on the order of 3×10^4 GM (Göppert-Mayer) and the local field enhancement effect [10], the

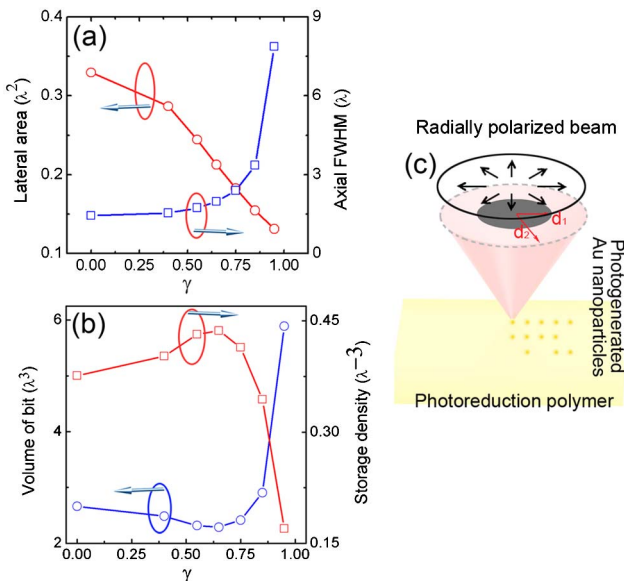


Fig. 1. (Color online) (a) The lateral area (red circles) and the axial FWHMs of the radially polarized beam (blue squares) as a function of γ . (b) The focal volume (circles) and the storage density limit (squares) predicted by the calculation are plotted as a function of γ . (c) Schematic illustration of the experimental configuration.

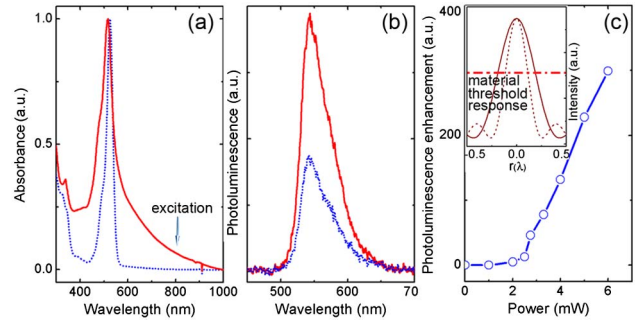


Fig. 2. (Color online) (a) Absorption and (b) fluorescence evolution after the laser irradiation. The arrow indicates the 2P excitation wavelength at 800 nm. The dotted blue and the solid red curves are the absorption and emission spectra before and after the laser irradiation, respectively. (c) The fluorescence intensity enhancement by the laser recording as a function of the writing power. The inset shows the schematic illustration of the SFV-enhanced threshold effect. The dashed and solid curves represent the cases with and without the SFV effect, respectively. The dot dashed curve indicates the material threshold response.

emission from R6G molecules is significantly enhanced and a bright spot can be recorded. When excited by a radially polarized beam using an annular objective of $\gamma = 0.65$, the SFV can introduce an enhanced threshold effect in recording. A sharp threshold effect starting from 2.5 mW can be recognized immediately when the photoluminescence enhancement is plotted as a function of the writing power, as shown in Fig. 2(c). The sharp increase in the fluorescence intensity in the photoreduction polymer is ideal for the application of superresolution recording combined with SFV-strengthened threshold response, as illustrated in the inset of Fig. 2(c).

The SFV together with the enhanced threshold effect can further lead to a focal spot smaller than that predicted by the calculation. The FWHM of the recorded

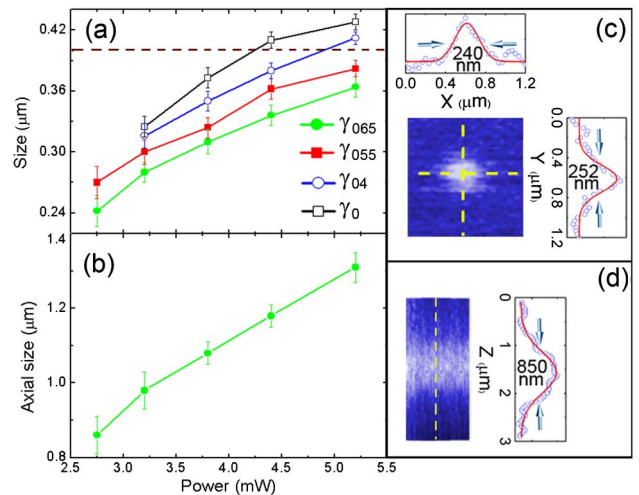


Fig. 3. (Color online) (a) FWHM plot of the average lateral sizes of 9 recorded bits as a function of the recording power. The dashed line indicates the diffraction limit. (b) FWHM plot of the axial response of bits recorded at $\gamma = 0.65$. (c) Confocal image of 1 bit at the threshold condition with a FWHM of 240 and 252 nm at the X and Y coordinates, respectively. (d) The axial image and the intensity plot of 1 bit with a FWHM of 850 nm.

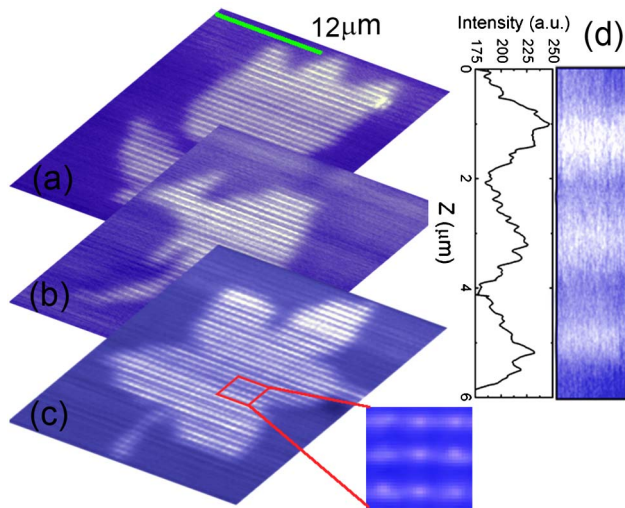


Fig. 4. (Color online) Demonstration of the $\lambda/3$ superresolution 3D optical recording by focusing a radially polarized beam using the annular objective of $\gamma = 0.65$. (a) Pattern tulip recorded in the first layer. (b) Pattern kangaroo recorded in the second layer. (c) Pattern leaf recorded in the third layer. The scale bar is $12\ \mu\text{m}$. The inset is the $1.8\ \mu\text{m} \times 1.8\ \mu\text{m}$ high magnification image of the area indicated by the square. (d) Axial image and the intensity plot of the three recorded layers.

bits was obtained by an average of nine recorded bits and plotted as a function of the recording power and γ , as shown in Fig. 3(a). The exposure time was kept at 25 ms. It depicts clearly that the enhanced longitudinal component, by increasing γ , can introduce a focal spot of the lateral size significantly below the diffraction limited barrier. The FWHM of the axial size recorded at $\gamma = 0.65$ was plotted as a function of the recording power in Fig. 3(b). The SFV-enhanced threshold recording at the optimized $\gamma = 0.65$ led to a fast shrink of the focal spot to a lateral FWHM of $245 \pm 20\ \text{nm}$ and an axial FWHM of $850 \pm 50\ \text{nm}$. The confocal image of 1 bit recorded at the threshold condition is shown in the inset of Fig. 3(c). The cross sections in the X and Y coordinates, indicated by the dashed lines, confirm the sharp focal spot of the lateral FWHM of $245 \pm 20\ \text{nm}$. This subwavelength resolution of $\lambda/3$ corresponds to a 45% reduction in the lateral size compared to the Airy focal spot limited by the diffraction. The axial image and the intensity plot of 1 bit are shown in Fig. 3(d), which has a FWHM of 850 nm. At the threshold condition, the focal volume of the annular objective of $\gamma = 0.65$ is thus reduced to $0.214\ \mu\text{m}^3$. This result corresponds to a 71% reduction in the focal volume compared to the diffraction limited Airy focal spot and permits a 320% enhancement in the storage density, which is highly desired for 3D optical data storage.

Figures 4(a)–4(d) demonstrate the application of such superresolution volume of the focal spot in multilayer optical data storage. Figures 4(a)–4(c) show the readout images of three patterns recorded at three layers with an annular aperture $\gamma = 0.65$. Each layer contains a pattern consisting of 40×40 bits with a bit spacing of $0.6\ \mu\text{m}$. The bit spacing is significantly reduced compared with

the linearly polarized beam recording where the bit separation was optimized at $1.6\ \mu\text{m}$ [19]. A pattern of tulip was recorded in the first layer while patterns of kangaroo and leaf were recorded in the second and third layers, respectively. A high magnification image of an area of 3×3 bit indicated by the square confirms the subdiffraction bit size. Three-layer information was recorded within six minutes. Ten layers of patterns can be recorded in a $20\ \mu\text{m}$ thick sample (data not shown here). Figure 4(d) shows the axial image and the intensity plot of the three recorded layers with a layer spacing of $2\ \mu\text{m}$. The storage density corresponds to an equivalent capacity of 3.0 Tbytes on a compact disk sized recording medium. This result is 120 times of that of the current Blu-ray Disc, which is the highest recording density reported.

In conclusion, we have experimentally demonstrated the superresolution recording by focusing a radially polarized beam with an annular objective. The enhanced threshold recording permits a 71% reduction of the focal volume compared to the diffraction limited Airy focal spot. Applying this superresolution focal spot in 2P induced 3D optical data storage in a photoreduction polymer has been demonstrated with an equivalent capacity of 3.0 Tbytes on a compact disk sized recording medium.

Min Gu thanks the Australian Research Council for its funding support through Laureate Fellowship scheme (FL100100099).

References

1. D. A. Parthenopoulos and P. M. Rentzepis, *Science* **245**, 843 (1989).
2. Y. Kawata, H. Ishitobi, and S. Kawata, *Opt. Lett.* **23**, 756 (1998).
3. D. Day, M. Gu, and A. Smallridge, *Opt. Lett.* **24**, 948 (1999).
4. A. Toriumi, S. Kawata, and M. Gu, *Opt. Lett.* **23**, 1924 (1998).
5. M. Watanabe, S. Juodkazis, H.-B. Sun, S. Matsuo, and H. Misawa, *Appl. Phys. Lett.* **77**, 13 (2000).
6. X. Li, J. W. M. Chon, R. A. Evans, and M. Gu, *Appl. Phys. Lett.* **92**, 063309 (2008).
7. M. Gu, *Advanced Optical Imaging Theory* (Springer, 2000).
8. D. Day and M. Gu, *Appl. Opt.* **37**, 6299 (1998).
9. X. Li, J. W. M. Chon, S. Wu, R. A. Evans, and M. Gu, *Opt. Lett.* **32**, 277 (2007).
10. P. Zijlstra, J. W. M. Chon, and M. Gu, *Nature* **459**, 410 (2009).
11. X. Li, J. W. M. Chon, R. A. Evans, and M. Gu, *Opt. Express* **17**, 2954 (2009).
12. S. Quabis, R. Dorn, M. Eberler, O. Glockl, and G. Leuchs, *Opt. Commun.* **179**, 1 (2000).
13. Q. Zhan and J. R. Leger, *Opt. Express* **10**, 324 (2002).
14. R. Dorn, S. Quabis, and G. Leuchs, *Phys. Rev. Lett.* **91**, 233901 (2003).
15. H. Wang, L. Shi, B. Lukyanchuk, C. Sheppard, and C. T. Chong, *Nat. Photon.* **2**, 501 (2008).
16. S. N. Kasarova, N. G. Sultanova, C. D. Ivanov, and I. D. Nikolov, *Opt. Mater.* **29**, 1481 (2007).
17. Y. Y. Cao, N. Takeyasu, T. Tanaka, X. M. Duan, and S. Kawata, *Small* **5**, 1144 (2009).
18. H. Kang, B. Jia, J. Li, D. Morrish, and M. Gu, *Appl. Phys. Lett.* **96**, 063702 (2010).
19. D. McPhail and M. Gu, *Appl. Phys. Lett.* **81**, 1160 (2002).